ELSEVIER

S0032-3861(96)00307-2

Polymer Vol. 37 No. 21, pp. 4675–4687, 1996

0032-3861/96/$15.00 + 0.00

Orientation determination and morphological study of high density polyethylene (HDPE) extruded tubular films: effect of processing variables and molecular weight distribution

Ta-Hua Yu and Garth L. Wilkes*
Department of Chemical Engineering, Virginia Polytechnic Institute and State University, Blacksburg, VA 24061, USA
(Received 6 November 1995; revised 3 February 1996)

The structure–property behaviour of high density polyethylene (HDPE) extruded tubular films having a blow up ratio of unity was investigated. Two different HDPE resins with identical $\bar{M}_n$ (14 600 g/mol) values but different distributions ($\bar{M}_w/\bar{M}_n$ = 10.3, 15.1) were utilized in this extrusion process. Systematic changes were also made in the process variables—these being the melt temperature at the die exit, the quench height, which is the distance from the exit of the die to the cooling ring, the flow rate of the air through the cooling ring, and the film line speed. The morphological features and state of orientation of the extruded tubular films were examined by transmission electron microscopy (TEM), high resolution scanning electron microscopy (HSEM), birefringence, wide and small angle X-ray scattering studies (WAXS, SAXS), and linear infra-red (i.r.) dichroism. A stacked lamellar or, in some cases, a fibril nucleated morphology was observed in the melt-extruded films by TEM. This technique clearly showed that the broader molecular weight samples possessed fibril nuclei that were not evident in the narrower molecular weight distribution films. The existence of the fibril nuclei was further confirmed from WAXS by the intense sharp spots superimposed on the equatorial (110), (200), and (020) reflections. The origin of this pronounced fibril nucleation was clearly believed to be due to the longer relaxation time behaviour of the broader distribution resin. The amorphous phase orientation and form birefringence for all films were found to be very small, and the observed birefringence arose almost exclusively from the crystalline phase. It was also found that the morphology and the orientation of the chain axis in the crystalline phase were particularly sensitive to the quench height and melt temperature for the narrower distribution HDPE films, but much less so for the broader distribution HDPE samples. Little dependence of structure/orientation was noted for either resin for the variables of the flow rate of the air through the cooling ring and the film line speed. These findings show the sensitivity of the molecular weight distribution to be a very important parameter, as are the specific processing variables of quench height and melt temperature, in determining the final solid state structure of the HDPE extruded tubular films. Copyright © 1996 Elsevier Science Ltd.

(Keywords: processing; polyethylene; fibril nucleation)

INTRODUCTION

Two important industrial processes, fibre spinning and extrusion, which result in preferred molecular orientation for semicrystalline polymers, have been investigated for many years on how the process variables can influence the final structure–property behaviour. The orientation of polymer chains as well as larger scale lamellar morphology are recognized as two principal variables in determining the performance and behaviour of final products. Considerable effort has been undertaken to define the relationship between the processing conditions and the structure and properties of extruded films, and to understand the fundamental aspects of the extrusion process such as the mechanism of molecular orientation during the processing, and the influence of molecular orientation on the crystallization and morphology of semicrystalline polymers. Until the work of Holmes *et al.* in the mid 1950s[1], there were no major published studies of the structures of extruded films. Using a Statton X-ray camera, Holmes *et al.*[1] examined the structures for melt extruded low-density polyethylene (LDPE) blown films and concluded that in this case, surprisingly, the a-axis of the unit cell lies along the extrusion direction, which was further confirmed by Aggarwal *et al.*[2], who showed that a strong short single (200) arc occurred along the machine direction in the X-ray diffraction pattern for a-axis orientation extruded film. They also concluded that the c-axis, the polymer chain direction, tended to orient perpendicular to the extrusion direction when a-axis orientation exists since the b-axis was found to preferentially lie along the

* To whom correspondence should be addressed

transverse direction. In 1954 Keller[3] raised an interesting concept of 'row orientation' in which the crystalline lamellar overgrowth occurs eptaxially from the c-axis oriented fibril. As the lamellae grow outwards, they gradually twist around the b-axis which stays perpendicular to the c-axis of the central fibril. The final orientation distributions obtained were that the b-axis lies mainly in the transverse direction–normal direction (TD–ND) plane, while the a- and c-axis are preferentially oriented along the machine direction (MD)[3,4]. Investigations into the orientation behaviour of crosslinked polyethylene were first carried out by Stein and Judge[5]. The crosslinked polyethylene prepared by irradiation was stretched with different stretch ratios and held in the stretched state for crystallization. The resulting orientation distributions determined by WAXS were found to vary from a-axis orientation to c-axis orientation as the stretch ratio was increased to a certain level. Using the method of pole figures for high-density polyethylene (HD) extruded films, Lindenmeyer and Lustig found support for row structure[6]. In 1967 Keller and Machin further modified the model of 'row nuclei' based on the level of stress for both LDPE and HDPE extruded films, and suggested that the row nucleated structure is similar to the 'shish-kebabs' crystallized from the stirred solution state[7]. Continuous investigations into the orientation behaviour of extruded blown films have been published by many people and the model of 'row nuclei' proposed by Keller *et al.* has been usually used to describe the structure for extruded blown films in the literature[8–13].

In the 1960s it was also found that within a certain range of processing conditions, spun fibres and uniaxially oriented extruded films of certain specific polymers showed high short-term recovery from nearly a 100% extension[14]. This property was termed 'hard elastic'[15], 'nonclassical elastic'[16], 'springy'[17], and 'energy elastic'[18]. The term 'hard elastic' is used most widely since the modulus of elasticity is much higher than that of classical elastic or rubbery polymers with similar recovery properties at strains less than 50% extension[19]. This type of hard elastic behaviour has been reported in polypropylene[15–18,20–22], polyoxymethylene copolymers[14], polyethylene[23,24], and nylon 66[25]. A stacked lamellae or, in some cases, a row nucleated morphology is formed when these polymers are melt-extruded and crystallized under stress[19]. Micropores can be produced in the melt-extruded films after annealing and stretching in the machine direction. This technique has been adopted to produce Celgard® microporous membranes (Hoechst Celanese Corporation) for blood oxygenation and battery separator applications[26–29]. It is believed that the orientation state and morphological features of the initial extruded films are important in controlling pore structure for microporous membranes. While there have been some studies investigating how to make microporous membrane using the hard elastic materials such as polypropylene[26–29], there has been little work carried out on polyethylene. Polyethylene has a rather simple crystallographic structure in that its unit cell is orthorhombic in nature with the chain axis lying along the c-axis. The techniques for characterizing different aspects of polyethylene have been well developed during the past half century. This suggests that polyethylene is an excellent candidate for studying the relationship between the processing conditions and the structure–property behaviour of extruded films, and for examining the mechanism of molecular orientation during the processing and the influence of molecular orientation on crystallization and morphology of semicrystalline polymers.

In this study two different HDPE resins with identical $\bar{M}_n$ (14 600 g/mol) values but different distributions ($\bar{M}_w/\bar{M}_n$ = 10.3, 15.1) were melt extruded through an annular die[30]. A blow-up ratio of 1.0 was used for producing essentially uniaxially oriented extruded tubular films, such as is used in making the microporous systems mentioned above. Since the structure–property behaviour of extruded HDPE films is dictated by the complex thermo-mechanical history experienced by the materials during fabrication, a number of variables including melt temperature at the exit of the die, quench location, quench rate, line speed and the nature of the die can affect the development of crystal orientation, lamellar morphology, degree of crystallinity and birefringence of extruded films. Because the resin molecular weight and its distribution is critical in controlling the rheological and associated relaxation behaviour, these variables also play an important role in the development of the orientation and final crystalline morphology in the films. In our study, the two HDPE resins were processed under controlled extrusion conditions. The morphological features and state of orientation in the HDPE extruded tubular films were examined by transmission electron microscopy (TEM), high resolution scanning electron microscopy (HSEM), birefringence, small and wide angle X-ray scattering studies (SAXS, WAXS), and Fourier transform infra-red (*FT*i.r.) dichorism. The degree of crystallinity of the extruded films was characterized by differential scanning calorimetry (d.s.c.). The objectives of this work are to investigate the relationships between selected resin variables and specific process variables on the inducement of molecular orientation during the processing as well as its influence on the crystalline morphology of these HDPE polymers.

The determination of chain orientation in polymers is of great interest from both a technical and a theoretical standpoint. The orientation distribution function of chain segments is rigorously defined by a series of spherical harmonic orientation functions. The second harmonic orientation function is known as the Herman's orientation function and given[31–33] by

$$f = \frac{(3\overline{\cos^2\theta} - 1)}{2} \tag{1}$$

in which θ is the angle between the chain axis and a chosen reference axis (usually the machine direction). When the polymer chains are aligned along the reference axis, i.e. $\theta = 0°$ for all chains, $f = +1$, whereas for the case of perpendicular orientation, i.e. $\theta = 90°$, $f = -1/2$. For random orientation it can be shown that $f = 0$. This function can be obtained from a number of spectroscopic techniques. Optical anisotropy or birefringence is one convenient way for measuring Herman's orientation function owing to the following equation

$$\Delta = \Delta^\circ * f \tag{2}$$

where Δ is the birefringence of the material under investigation and Δ° is the birefringence of the fully

oriented material[34]. However, in the case of semicrystalline polymers, the crystalline and amorphous chain orientation must be investigated separately. Assuming the expected additivity of the two contributions to the total birefringence, Stein proposed the following relationship for semicrystalline polymers above the glass transition temperature (T_g) where distortion or glassy birefringence should not exist

$$\Delta = X_c * f_c * \Delta_c^\circ + (1 - X_c) + f_{am} * \Delta_{am}^\circ + \Delta_{form} \quad (3)$$

Here, f_c and f_{am} are the crystalline and amorphous orientation functions, Δ_c° and Δ_{am}° are the intrinsic birefringence values for the perfectly oriented crystalline and amorphous phases, X_c is the crystal volume fraction, and Δ_{form} is the form birefringence due to the distortion of the electric field of the incident light wave at the phase boundary of anisotropic structure such as stacked lamellae[34]. This latter contribution is recognized to generally be very small and therefore often neglected, but we will address this further below. For polyethylene the value $\Delta_c^\circ = 0.058$ has been universally accepted[35] and the amorphous birefringence is $\Delta_{am}^\circ = 0.200$ which is an average value from several sources in the literature[36–39]. Internal field effects in the crystalline phase result in a much smaller crystalline intrinsic birefringence than that for the amorphous phase, as has been discussed by Mead *et al.*[38].

The coordinate system for describing the crystal orientation of the unit cell of HDPE is shown in *Figure 1*[40,41]. The angles α, β, and ϵ are measured between the z axis (the machine direction) and the a, b, and c crystallographic axes. Since the three axes are perpendicular for the orthorhombic unit cell,

$$\cos^2\alpha + \cos^2\beta + \cos^2\epsilon = 1 \quad (4)$$

so

$$f_a + f_b + f_c = 0 \quad (5)$$

where the three axial orientation functions are defined as

$$f_a = \frac{(3\overline{\cos^2\alpha} - 1)}{2} \quad (6)$$

$$f_b = \frac{(3\overline{\cos^2\beta} - 1)}{2} \quad (7)$$

$$f_c = \frac{(3\overline{\cos^2\epsilon} - 1)}{2} \quad (8)$$

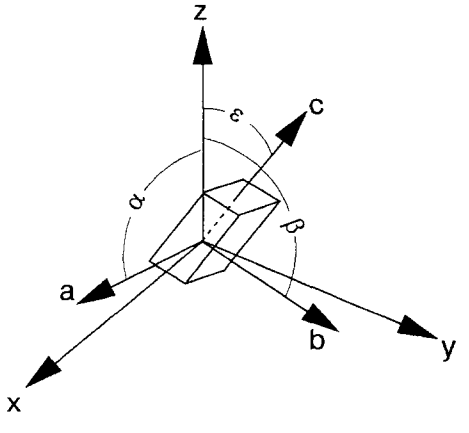

Figure 1 The coordinate system used for describing the orientation of a polyethylene crystal

These three functions are not independent and only two of them are necessary in order to completely specify the orientation. For uniaxially oriented polyethylene, it is more convenient to work with the (200) and (020) reflections. The angles, measured from the equator to a point on these reflections, are designated as ψ_{200} and ψ_{020}. The orientation functions of the crystals are then given by

$$f_a = \frac{(3 * \cos^2\theta_{200} * \overline{\sin^2\psi_{200}} - 1)}{2} \quad (9)$$

$$f_b = \frac{(3 * \cos^2\theta_{020} * \overline{\sin^2\psi_{020}} - 1)}{2} \quad (10)$$

where θ_{200} and θ_{020} are the Bragg angles for the two reflections. The value of $\sin^2\psi$ may be approximated from the half width of the appropriate reflection arcs[35,40,41].

The orientation functions of crystal axes a and b may also be evaluated from the *FT*i.r. dichroic ratios, D, for the 730 and 720 cm^{-1} bands, D_{730} and D_{720}, by the following relations[42–45]

$$f_a = \frac{(D_{730} - 1)}{(D_{730} + 2)} \quad (11)$$

$$f_b = \frac{(D_{720} - 1)}{(D_{720} + 2)} \quad (12)$$

Once f_a and f_b are evaluated, f_c can be calculated using equation (5). There are some difficulties, however, in using *FT*i.r. dichroism for determining f_a and f_b, as has been discussed by past workers[43–46]. (In the work to be discussed shortly, the values of f_c evaluated from WAXS will be compared to those calculated from *FT*i.r. dichroism. Through the use of the birefringence measurements in conjunction with WAXS and *FT*i.r. dichroism results, it will be shown that WAXS produces a more accurate result for f_c than does *FT*i.r. dichroism.) Since the transition moment associated with the 1368 cm^{-1} band is perpendicular to the chain axis, the amorphous orientation function, f_{am}, can also be evaluated from *FT*i.r. dichroism using the amorphous band at 1368 cm^{-1} by[47,48]

$$f_{am} = \frac{(D_{1368} - 1)}{(D_{1368} + 2)} \quad (13)$$

Considerable effort has been devoted to studying the microstructure of hard elastic extruded films using electron microscopy techniques[15,49–51]. The row nucleated lamellar structure proposed by Keller and Machin[7] is accepted in many studies as a common feature to the hard elastic extruded films. Keller and Machin proposed that fibril nucleation is essential for crystallization under stress[7]. Under low stress during crystallization, the twisted lamellae grow from the central fibril nucleus to form winding ribbon-like structure while crystallization under high stress produces stacks of flat planar lamellae extended from the central fibril nucleus that is itself highly aligned along the principal stress axis (generally the MD). The latter will result in a c-axis orientation diffraction pattern while the low stress case will give signs of a-axis orientation. In a recent review article[52], the coil → stretching transition concept initially addressed by de Gennes[53] was used by

Keller *et al.* to explain the orientation–crystallization behaviour of polymer melt during processing. Keller *et al.* pointed out that for the row nucleated structure, the fibril nuclei and lamellar platelet components are indistinguishable by the usual wide angle X-ray diffraction (WAXD) pattern. The explanation is that for crystallization under high stress, the crystallographic orientation of the central fibril nuclei will always impart a c-axis orientation parallel to the flow direction and the transverse flat lamellae, which are parallel to each other, will also display c-axis orientation with respect to the flow direction thereby not allowing separation of these two respective oriented structures by WAXS. On the other hand for crystallization under low stress, the amount of fibril nuclei is so small that the transverse lamellae will twist and display some a-axis behaviour in the diffraction pattern. In the work presented here the authors will show that two different morphologies, stacked lamellae and fibril nucleated structure, are observed in the extruded HDPE films. The corresponding fibril nuclei and lamellar platelet components of the row nucleated samples are clearly distinguishable in some cases by WAXD. The formation of this morphology, either a pure stacked lamellae or row nucleated structure, depends on the molecular weight distribution of the resin, and is therefore dependent on the melt relaxation/crystallization behaviour of the specific polymer during the cooling procedure following extrusion.

EXPERIMENTAL

Two commercial HDPE resins, designated as Resins 1 and 2 were employed in this study. Their molecular weight characteristics which were determined by gel permeation chromatography (g.p.c.) at 135°C in 1,2-dichlorobenzene are listed in *Table 1*. These two resins were melt extruded through an annular die under controlled processing conditions. The process variables investigated are marked on the schematic of the extrusion operation in *Figure 2*. Four main processing parameters: the melt temperature, T_{melt}, at the die exit, the quench height, which is the distance from the exit of the die to the cooling ring, the flow rate of the air through the cooling ring, and the line speed are listed in *Tables 2* and *3*. The process variables included in *Tables 2* and *3* were chosen for two reasons: 1) the extrusion process can not be operated successfully for certain process conditions and therefore it is impossible to cover a wide processing window; and 2) the range of the data in *Tables 2* and *3* were developed for statistical analysis in order to minimize the number of extrusion runs. It is to be noted that in this study where uniaxial behaviour is desired, no expansion of the tubular film occurred, i.e. the blow up ratio was 1.0. This is in great contrast to the usual blown film processes where balanced biaxial behaviour is generally desired.

Table 1 Molecular weight features of HDPE resins utilized

Sample	$\bar{M}_n$ (g mol^{-1})	$\bar{M}_w$ (g mol^{-1})	$\bar{M}_w/\bar{M}_n$
Resin 1	14 600	150 000	10.3
Resin 2	14 600	219 000	15.1

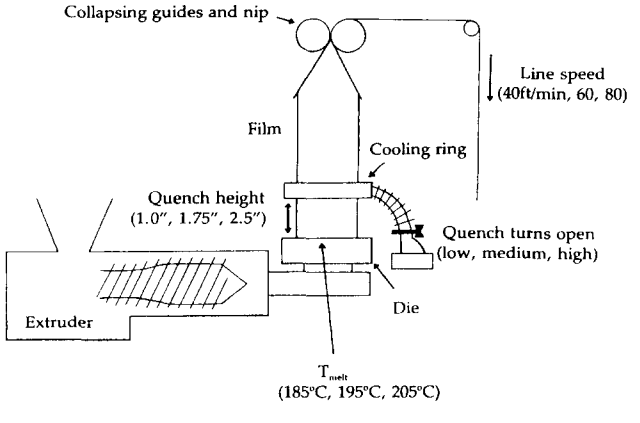

Figure 2 A schematic of the extrusion process

Table 2 Summary of extrusion variables for Resin 1

Sample	Melt temperature (°C)	Quench height (inch)	Air flow rate in air ring	Line speed (ft min^{-1})
A1	205	2.5	low	40
A2	205	2.5	high	80
A3	195	1.75	medium	60
A4	185	2.5	low	80
A5	195	1.75	medium	60
A6	205	1.0	high	40
A7	185	2.5	high	40
A8	205	1.0	low	80
A9	185	1.0	low	40
A10	185	1.0	high	80

Table 3 Summary of extrusion variables for Resin 2

Sample	Melt temperature (°C)	Quench height (inch)	Air flow rate in air ring	Line speed (ft min^{-1})
B1	205	2.5	low	40
B2	205	1.0	high	40
B3	195	1.75	medium	60
B4	205	2.5	high	80
B5	185	2.5	high	40
B6	195	1.75	medium	60
B7	185	2.5	low	80
B8	205	1.0	low	80
B9	195	1.75	medium	60
B10	185	1.0	high	80
B11[a]	195	1.75	medium	60

[a] Processed with different die gap

A Babinet compensator method was used to measure the film birefringence 24 h after extrusion. The effect of the introduction of organic liquids of different refractive index on the birefringence of the extruded films was measured using the procedures developed by Bettelheim and Stein[54] for purpose of determining if any significant form birefringence occurred. The organic solvents used in this work were carbon tetrachloride with refractive index = 1.4607, benzene with refractive index = 1.5014, chlorobenzene with refractive index = 1.5250, and trichlorobenzene with refractive index = 1.5671.

The degree of crystallinity, X_c, of the samples was determined from the heat of fusion using a Seiko d.s.c. at a heating rate of 10°C min^{-1}. The fractional crystallinity (mass fraction) X_c was calculated based on d.s.c. data

according to the equation

$$X_c = \frac{\Delta H}{\Delta H_0} \tag{14}$$

where ΔH_0 is the specific heat of melting of an ideal crystal. For polyethylene (PE), the commonly accepted value of $\Delta H_0 = 293\,J\,g^{-1}$ has been used in this study[55].

The crystalline orientation of the films was studied by WAXS using a Philips table-top X-ray generator model PW1170 equipped with a standard vacuum sealed Warhus photographic pinhole camera. The method of determining the value of f_c of the chain orientation function in the crystalline phase with WAXS was discussed in the previous section and will not be repeated here. A Nicolet 510 *FT* i.r. spectrometer equipped with a polarizer was used for determining *FT* i.r. dichroism. The absorption bands at 730 and 720 cm^{-1} were used to calculate the values of f_a and f_b. The absorption band at 1368 cm^{-1} was used to calculate the orientation function, f_{am}, of the amorphous phase.

Samples for TEM studies were first treated with chlorosulfonic acid[56] at 60°C for 6 h before microtoming. Thin sections were normally stained on the TEM grid with a dilute aqueous solution of uranyl acetate and then examined by a Philips EM-420 scanning transmission electron microscope (STEM) operated in the transmission mode at 100 kV. Samples for HSEM analysis were coated with a thin layer of gold and then examined by the same STEM but operated in the scanning mode at 100 kV.

SAXS experiments were performed using Ni-filtered CuK_α radiation ($\lambda = 1.54$ Å) on a compact Kratky camera with slit geometry, equipped with a Braun position sensitive detector. No desmearing of the intensity data was undertaken for this investigation. After the corrections for parasitic scattering and absorption, the scattering curves were normalized to the main beam intensity and sample thickness. The results were plotted against the angular variable, $s = 2(\sin\frac{\theta}{2})/\lambda$ where θ is the radial scattering angle.

Thermal shrinkage determination for the extruded films were done by observing the length difference between two marks labelled on the sample surface along the machine direction before and after annealing in an oven at 105, 120, and 125°C for 30 min. The percent (%) shrinkage is defined by:

$$(\%)\ \text{shrinkage} = \frac{(L_i - L_f)}{L_i} * 100 \tag{15}$$

where L_i is the initial length between the two marks and L_f is the final length between the two marks following thermal treatment.

RESULTS AND DISCUSSION

The TEM micrographs obtained from three orthogonal directions—along the TD, along the MD, and along the ND of the highest oriented extruded film made from the narrower molecular weight material—Resin 1 (sample A10) are shown in *Figure 3*. Stacked lamellae without fibril nuclei were observed from the micrographs viewed along the TD and the ND. The lamellae viewed along the TD look somewhat more 'corrugated' than those viewed along the ND. Since the micrograph viewed along the MD was microtomed across the surface of stacked lamellae, it is not surprising that one would not see well defined structures along this direction. The so called 'fibril nuclei' which have been recognized as a common

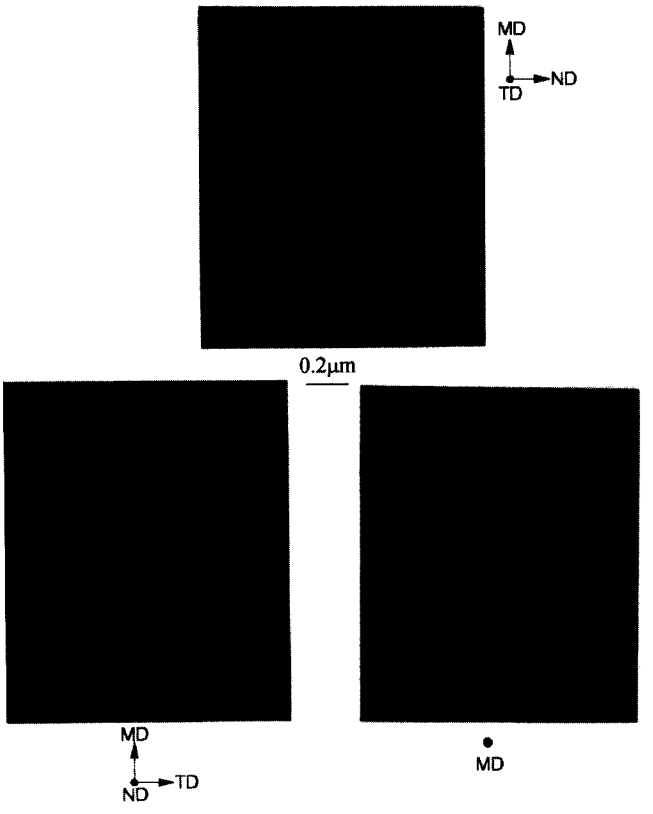

Figure 3 The TEM micrographs for the highest oriented Resin 1, sample A10. The TD, MD, and ND directions are shown as labelled

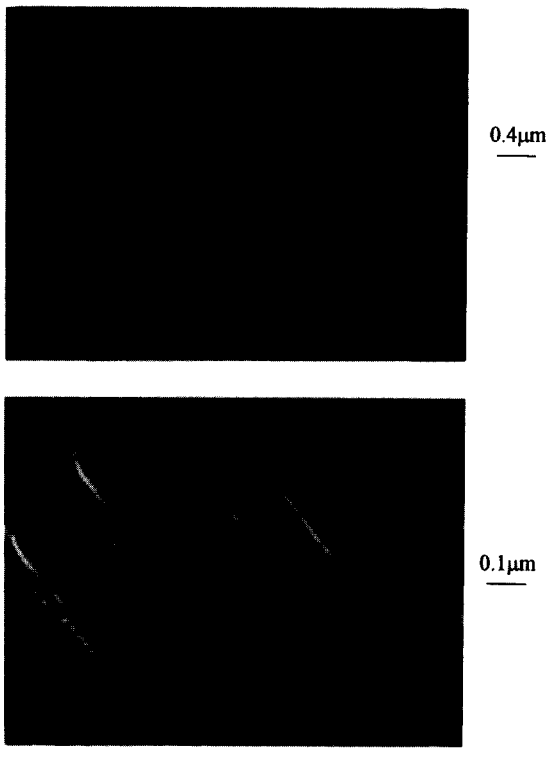

Figure 4 The HSEM micrographs for the highest oriented Resin 1, sample A10

characteristic for extruded film cannot be seen in *Figure 3*. The HSEM micrographs in *Figure 4* taken on the surface of the sample appear to have thicker lamellae than the TEM micrographs in *Figure 3*. Microcracks can be seen in *Figure 4* but not in *Figure 3*. The radiation damage from the electron beam on the sample surface is the cause of the microcracks in *Figure 4*. The thickness of the gold coating on the sample surface, used to minimize surface changing, will affect the observed lamellae thickness, and thus it is not surprising to see that *Figure 4* indeed shows thicker lamellae than *Figure 3*. Another possible explanation for the discrepancies between HSEM and TEM is that the structure on the surface of the extruded film is somewhat different from the structure in the bulk of the film and also direct differentiation of the interlamellar amorphous layer can not be made by HSEM. If so, TEM would be a better tool for characterizing the bulk structure in the extruded films. The TEM micrograph viewed along the TD in *Figure 5* shows a structure very close to the surface of the extruded film. Due to the thin film thickness (about 1 ml) of the extruded film, no distinct skin-core morphological differences were seen for this or any other sample as well.

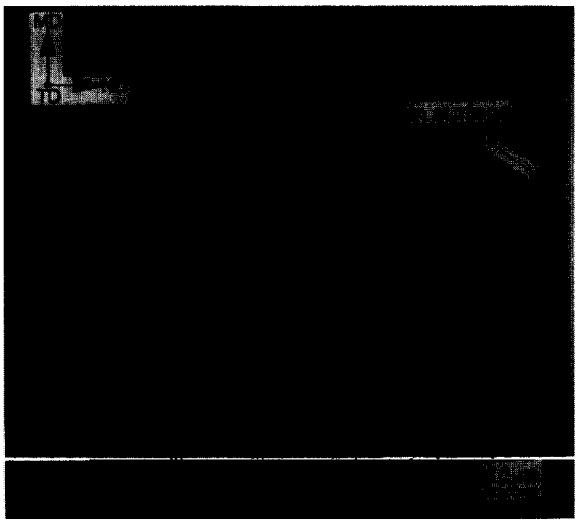

Figure 5 The TEM micrograph of the highest oriented Resin 1, sample A10. This micrograph shows the morphology very close to the film surface

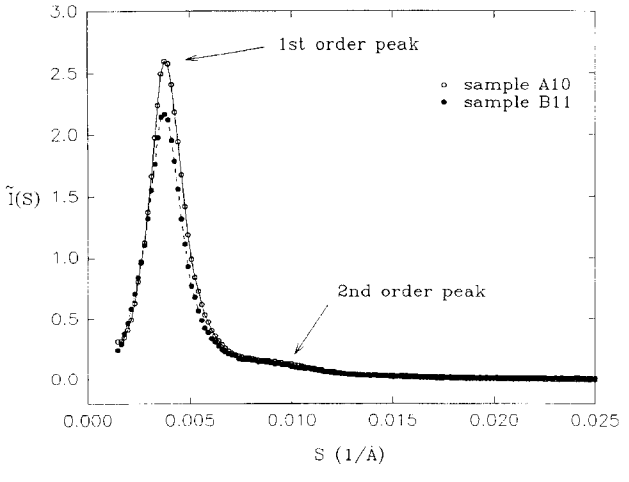

Figure 6 The slit smeared SAXS spectra from the highest oriented Resin 1 sample A10, and Resin 2 sample B11

In *Figure 6*, the corresponding SAXS profile of sample A10 (Resin 1) is given for the slit-smeared intensity vs scattering vector, s, as defined earlier. The corresponding SAXS profile of the highest oriented sample for Resin 2 (sample B11) is also shown for comparison—the latter of which will be addressed later in this paper. Both SAXS profiles were obtained by passing the beam along the normal direction and obtaining the scan along the MD. As might be expected, these two profiles clearly show a very well defined first order peak along with a much weaker secondary peak. Clearly, these data strongly support the TEM observations that a well stacked lamellar structure is generated in these film materials. It should again be pointed out that, since the data are 'slit smeared', the second order scattering peak is somewhat less distinct than it would be had a desmearing analysis been applied. It might also be mentioned that similar SAXS profiles were obtained from all of the extruded films and further comments regarding these SAXS profiles will be addressed later.

The WAXS pattern in *Figure 7* was obtained by aligning the MD of the sample in *Figures 3* and *4* to be parallel to the X-ray beam. Complete rings for the various reflections in *Figure 7* show that the extruded film is essentially uniaxially oriented along the MD and suggests that one can use a flat film X-ray camera to approximate the orientation state of the extruded films produced in this study according to the procedures outlined earlier. In the following section, the WAXS diffraction patterns for both Resin 1 and Resin 2 were obtained by exposing the extruded films along the ND of the extruded films and the results were utilized to determine f_c by equations (5), (9) and (10).

The WAXS diffraction patterns for specific extruded films of Resin 1 are shown in *Figure 8*. These samples as designated earlier in *Table 2* are: sample A1 with process conditions: $T_{melt} = 205°C$, quench height = 2.5″, air flow rate = low, and line speed = 40 ft min^{-1}, sample A7 with process conditions: $T_{melt} = 185°C$, quench height = 2.5″, air flow rate = high, and line speed = 40 ft min^{-1}, and sample A10 with process conditions: $T_{melt} = 185°C$, quench height = 1.0″, air flow rate = high, and line speed = 80 ft min^{-1}. The values of f_c calculated from

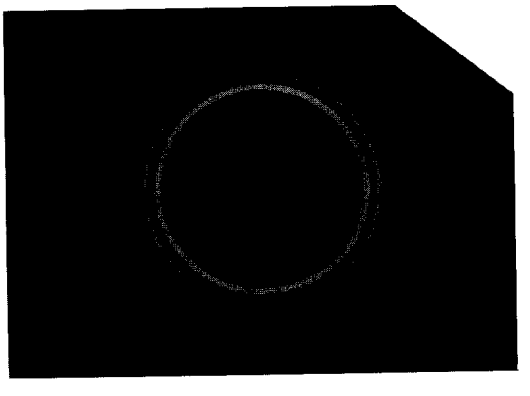

Figure 7 The WAXS diffraction pattern for the sample in *Figure 3*. The X-ray beam was along the MD

Table 4 The orientation functions, measured birefringence and degree of crystallinity of Resin 1

Sample	$f_{c,WAXS}$	$f_{c,i.r.}$	f_{am}	Δ_T	T_m (°C)	X_c
A1	0.45	0.27	−0.01	0.0149	137.0	0.59
A2	0.46	0.28	0.01	0.0152	137.0	0.60
A3	0.50	0.32	−0.03	0.0183	136.9	0.56
A4	0.51	0.33	0.05	0.0193	135.9	0.59
A5	0.56	0.37	−0.01	0.0191	136.7	0.58
A6	0.57	0.38	0.03	0.0204	136.7	0.57
A7	0.60	0.40	0.03	0.0206	138.0	0.59
A8	0.60	0.45	0.07	0.0228	136.4	0.61
A9	0.66	0.49	0.04	0.0265	137.7	0.57
A10	0.67	0.51	0.03	0.0272	137.5	0.59

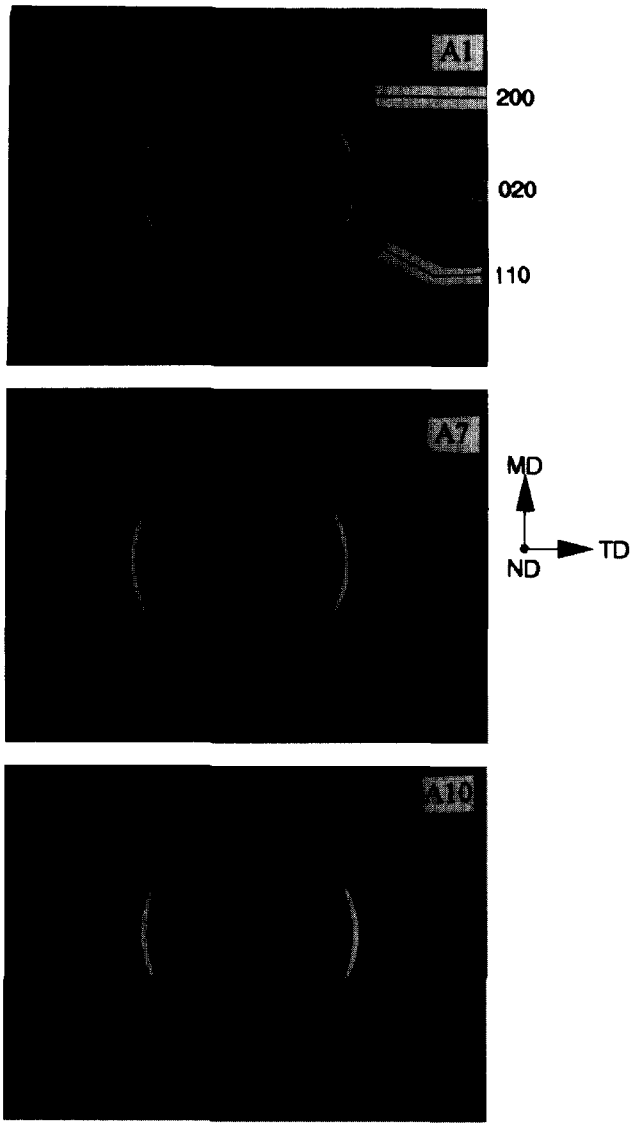

Figure 8 The WAXS diffraction patterns for samples A1, A7, and A10 made from Resin 1. The X-ray beam was along the ND

these diffraction patterns are listed in *Table 4*. The split 200 and 110 reflections are clearly shown for the lowest oriented sample A1 with $f_c = 0.45$, thereby providing an average orientation angle, $\langle\theta\rangle$, of 37°. The reflections start merging toward the equatorial direction with increasing f_c and completely merge together along the equator for the sample A10 which has the highest f_c value, 0.67 ($\langle\theta\rangle = 28°$). On the other hand, the b-axis

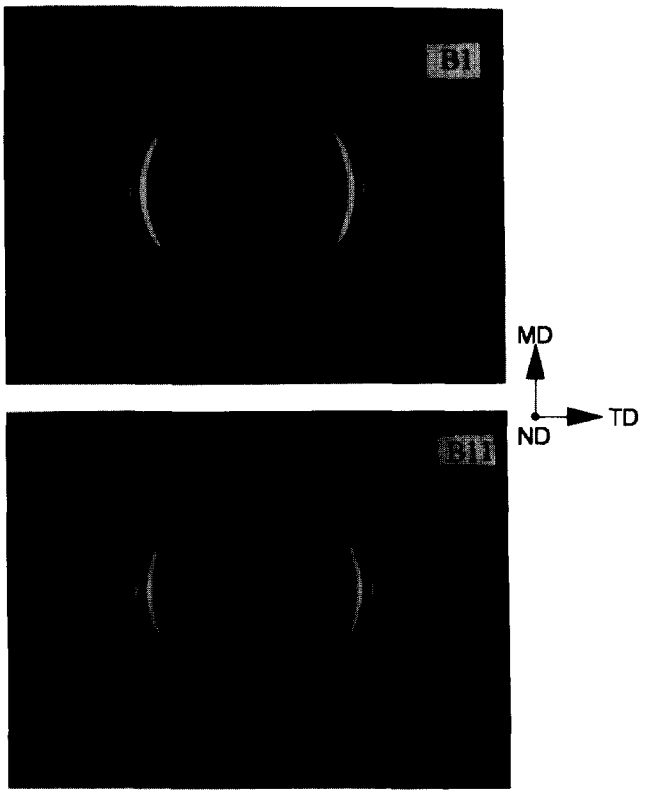

Figure 9 The WAXS diffraction patterns for samples B1 and B11 made from Resin 2. The X-ray beam was along the ND

((020) reflection) lying along the equator does not show much change for the samples made from Resin 1 in *Figure 8*. This could be due to the intensity of the (020) reflection being rather low and hence it is more difficult to follow the variation of the orientation for (020) reflection using the flat film camera technique. These observations suggest that the melt extrusion process variables can significantly influence the crystalline orientation state of the extruded films made from the narrower distribution Resin 1. In *Figure 6*, besides the intense 'split' reflections, there is some sign of a-axis orientation along the meridional direction. *Figure 9* provides the diffraction patterns for the lowest ($f_c = 0.62$, $\langle\theta\rangle = 30°$) and highest ($f_c = 0.72$, $\langle\theta\rangle = 26°$) oriented samples of the extruded films made from Resin 2. Comparing these data with results from Resin 1, none of the films made from Resin 2 display a split in the (200) and (110) reflections. In addition, *Figure 9* also shows that intense sharp spots are found superimposed on the equatorial (110), (200), and (020) reflections that do not exist in *Figure 8*. The cause for the intense sharp spots will be discussed later. The values of f_c for Resin 2 were calculated without considering the existence of these particularly intense sharply azimuthally dependent equatorial spots and are listed in *Table 5*. Comparing the results for samples A1 and B1, it is clear that under exactly the same extrusion process conditions, the film made from Resin 2 with a broader molecular weight distribution has a distinctly higher value for f_c than the film made from Resin 1. Unlike Resin 1, *Figure 9* also suggests that the values of f_c of the samples made from Resin 2 are less sensitive to the processing variables utilized. A small amount of intensity for the (200) reflection along the MD is also noticed for Resin 2.

Table 5 The orientation functions, measured birefringence and degree of crystallinity of Resin 2

Sample	$f_{c,WAXS}$	$f_{c,i.r.}$	f_{am}	Δ_T	T_m (°C)	X_c
B1	0.62	0.45	0.04	0.0195	134.9	0.64
B2	0.65	0.48	0.04	0.0245	136.2	0.66
B3	0.66	0.49	0.02	0.0246	136.3	0.59
B4	0.66	0.49	0.01	0.0238	136.2	0.62
B5	0.55	0.50	0.04	0.0268	136.3	0.64
B6	0.66	0.51	0.02	0.0244	135.6	0.65
B7	0.67	0.51	0.04	0.0264	136.6	0.63
B8	0.68	0.52	0.04	0.0258	136.6	0.66
B9	0.69	0.52	0.03	0.0274	135.8	0.61
B10	0.69	0.54	0.01	0.0275	135.6	0.60
B11	0.72	0.56	0.04	0.0295	135.6	0.63

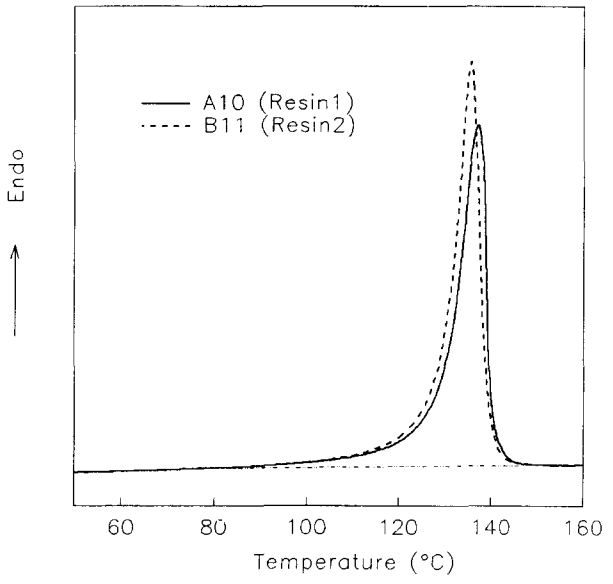

Figure 10 The d.s.c. scans for samples, A10 (Resin 1) and B11 (Resin 2)

According to the row nucleated model, this could be from a small amount of lamellae twist in the extruded films. Since our extensive TEM analysis did not show the sign of lamellae twist, the answer for the a-axis orientation along the MD is still not entirely clear.

Figure 10 shows the d.s.c. scans for the highest oriented Resin 1 and 2. A single rather sharp melting peak was observed for both resins. The melting temperature and degree of crystallinity measured by d.s.c. are included in *Tables 4* and *5*. For all processed films, the degree of crystallinity of Resin 2 is approximately 5% higher than that of Resin 1. This difference is believed due to the fact that the broader distribution Resin 2 has a longer melt relaxation time behaviour than the narrower distribution Resin 1. During the extrusion process, Resin 2 is more readily oriented than Resin 1 and the stress-induced crystallization which is strongly dependent on molecular orientation allows Resin 2 to achieve a higher degree of crystallinity than Resin 1. This observation of the effect of molecular weight distribution on the crystallization behaviour of HDPE under orientation matches well with what was observed for polypropylene by Misra *et al.*[57]. The variation of melting temperature and degree of crystallinity is small within either resin and this suggests

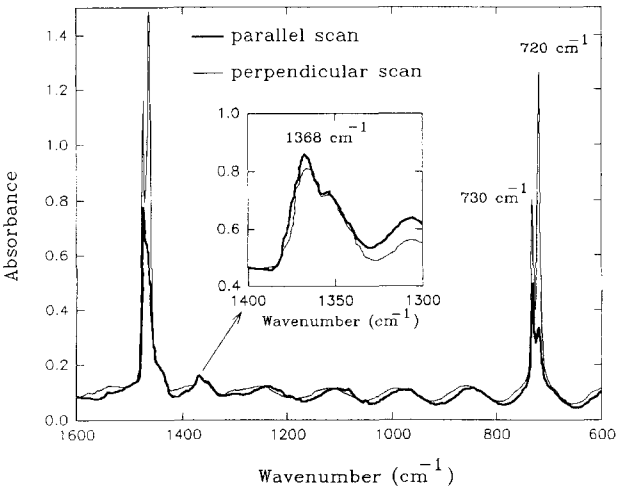

Figure 11 The *FT*i.r. spectra of parallel and perpendicular scans for the 720, 730, and 1368 cm^{-1} bands obtained on sample A10

Table 6 *FT*i.r. dichroic ratios determined for Resin 1

Sample	D_{720}	D_{730}	D_{1368}
A1	0.309	1.09	0.964
A2	0.306	1.07	1.030
A3	0.294	0.959	0.924
A4	0.297	0.93	1.150
A5	0.247	0.896	0.967
A6	0.285	0.801	1.110
A7	0.288	0.752	1.100
A8	0.268	0.655	1.240
A9	0.269	0.560	1.120
A10	0.247	0.549	1.120

Table 7 *FT*i.r. dichroic ratios determined for Resin 2

Sample	D_{720}	D_{730}	D_{1368}
B1	0.280	0.655	1.120
B2	0.266	0.588	1.120
B3	0.261	0.575	1.070
B4	0.273	0.562	1.040
B5	0.264	0.564	1.130
B6	0.261	0.542	1.050
B7	0.262	0.542	1.130
B8	0.271	0.500	1.120
B9	0.259	0.510	1.100
B10	0.247	0.486	1.020
B11	0.254	0.439	1.130

that both properties are not greatly affected by the process variables utilized in this work.

An example of the parallel and perpendicular *FT*i.r. absorption spectra for the extruded polyethylene films are shown in *Figure 11*. The dichroic ratios for the 720, 730, and 1368 cm^{-1} bands calculated from the *FT*i.r. spectra are listed in *Tables 6* and *7*. The anisotropic effect increases as the dichroic ratio for the specific transition moment deviates from 1. Therefore *Tables 6* and *7*, the 730-cm^{-1} band show more orientation than does the 720-cm^{-1} band and the transition moment corresponding to the 1368-cm^{-1} band is almost randomly distributed in the extruded films. The crystalline orientation function $f_{c,i.r.}$ and amorphous orientation function f_{am} calculated from the dichroic ratios in *Tables 6* and *7* are

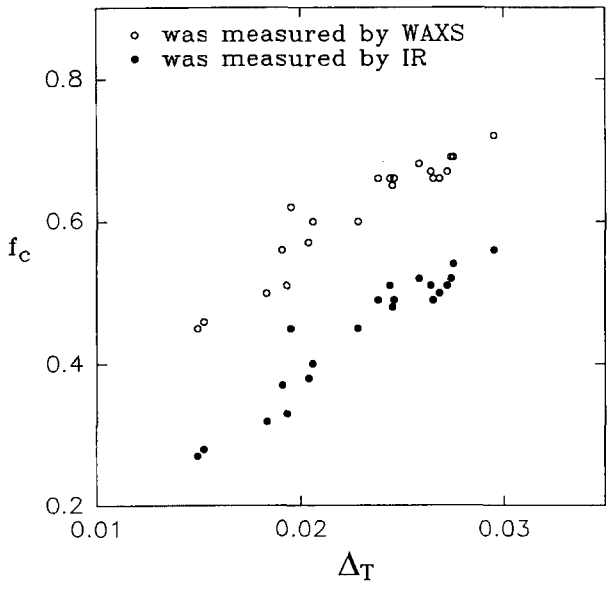

Figure 12 The crystalline orientation function, f_c, measured by WAXS as well as by i.r. *versus* the measured birefringence, Δ_T

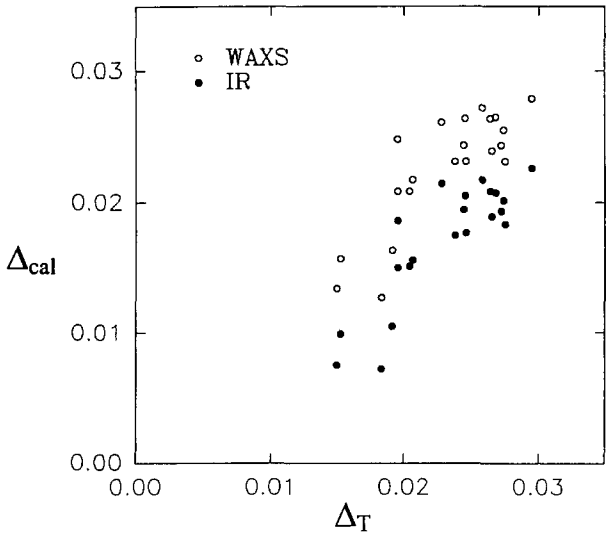

Figure 13 The calculated total birefringence plotted against the measured birefringence

listed in *Tables 4* and *5*. The data in *Tables 4* and *5* show that the values of $f_{c,i.r.}$ are systematically smaller than the corresponding values of $f_{c,WAXS}$. Also, the amorphous phase orientation, f_{am}, is very small (close to 0) for all samples. The f_c values calculated from WAXS and *FT*i.r. for the samples made from both Resin 1 and 2 are plotted against the measured birefringence, Δ_T, in *Figure 12* where a linear relationship between f_c and Δ_T is observed. Neglecting form birefringence effects, as we have justified, one can then calculate the birefringence for the extruded films using equation (3). The calculated birefringence, Δ_{cal}, is plotted vs the experimentally determined birefringence, Δ_T, in *Figure 13*. This figure shows that the birefringence value, $\Delta_{cal,WAXS}$, calculated from the $f_{c,WAXS}$ determined by WAXS matches much better with the measured birefringence, Δ_T, than that calculated from the $f_{c,i.r.}$ determined by i.r. dichroism. This result strongly suggests that WAXS analysis gives a

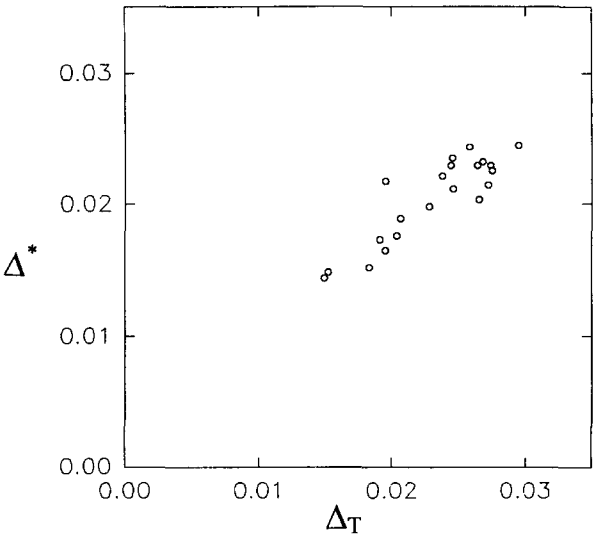

Figure 14 The birefringence calculated from the crystalline phase orientation (as determined by WAXS) plotted against the measured birefringence

more accurate value of f_c than *FT*i.r. Several studies have discussed the discrepancies of using *FT*i.r. to determine the crystalline orientation function[43–46]. To summarize, the discrepancies can be from: 1) the uncertainty about the precise direction of the transition moments with respect to the a and b axes[44]; 2) the close overlap of the two peaks, 720 and 730 cm^{-1}, and the presence of a broad amorphous component centered at 720 cm^{-1} which may contribute unequally to both peaks[43–45]. *Tables 4* and *5* also show that the amorphous orientation obtained from the 1368 cm^{-1} absorption band was very small so that the observed birefringence should arise almost exclusively from the crystalline phase. Indeed, if one calculates the birefringence using the following equation:

$$\Delta^* = X_c * f_{c,WAXS} * \Delta_c^0 \qquad (16)$$

and plots Δ^* vs the measured birefringence, Δ_T, as shown in *Figure 14*, the latter statement is well verified. That is, the deviation of the points from the 45° diagonal line is small. It indicates that the Δ^* calculated only from the contribution of the crystalline phase in general matches well with the measured birefringence and further supports the assumption that the form birefringence is small.

In 1958, Stein *et al.* showed that an appreciable amount of form birefringence was observed for stretched polyethylene films[55]. They suggested that the observed form birefringence results from aggregates of crystals and amorphous material which orient at a faster rate than the crystals themselves and therefore amorphous birefringence (orientation) could not be neglected. A similar study was done by Noether *et al.* for elastic polypropylene fibres[58]. In their study[58], form birefringence was found significant for the stretched porous fibres but not for the unstretched fibres. Noether *et al.* pointed out that the observed form birefringence in the stretched fibres was due to the geometrically anisotropic voids produced by the stretching process. Similar to what was found by Noether *et al.* for unstretched polypropylene fiber having a stacked lamellar structure, the form

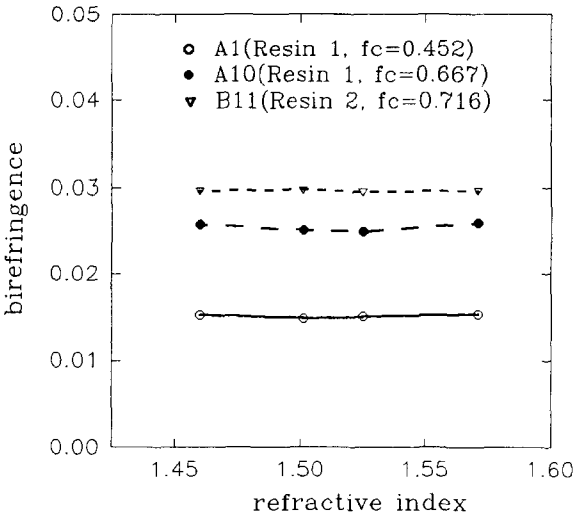

Figure 15 The form birefringence of samples A1, A10, and B11 plotted against the refractive index of the swelling organic liquids

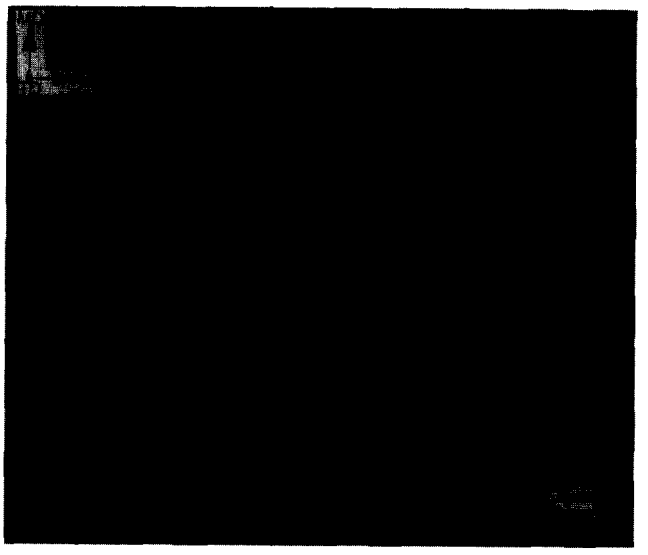

Figure 17 The TEM micrograph of highest oriented Resin 1, sample A10

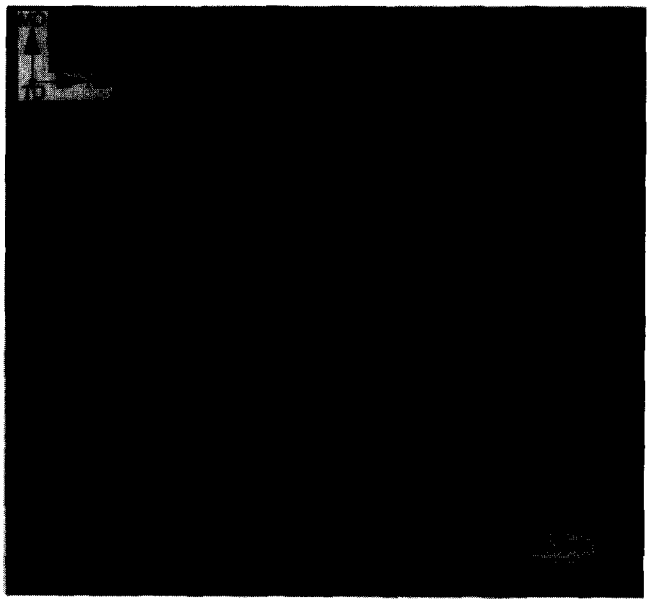

Figure 16 The TEM micrograph of the lowest oriented Resin 1, sample A1

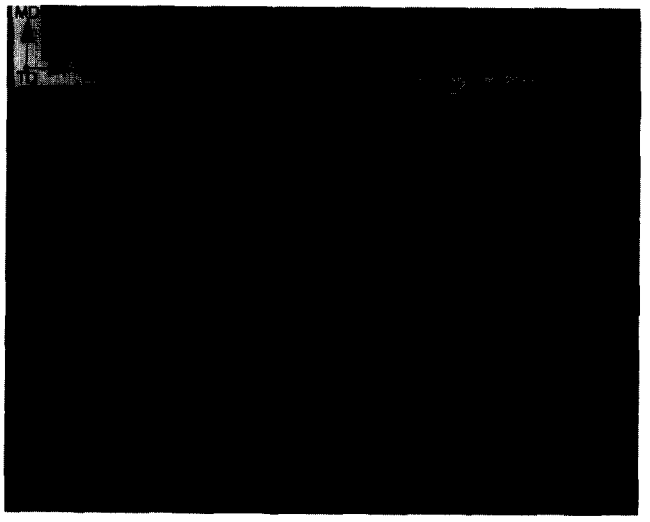

Figure 18 The TEM micrograph of the lowest oriented Resin 2 film—sample B1

birefringence was shown to be very small for both Resin 1 and Resin 2 in *Figure 15*. This finding further proves the assumption that form birefringence can be neglected. Since *FT*i.r. dichroism shows that the amorphous orientation is small, if one anneals the extruded films at temperatures higher than the α transition of polyethylene they should not shrink at higher temperature. Indeed from the shrinkage analysis of the lowest and highest oriented films of both Resin 1 and Resin 2, the maximum shrinkage obtained was found to be less than 2.5%. This observation reveals that the extruded films made from both resins have negligible shrinkage along the machine direction and also further confirms the *FT*i.r. analysis of the 1368 cm^{-1} band.

The TEM micrograph of the lowest oriented sample, A1, of the films made from Resin 1 is shown in *Figure 16*. The stacked lamellae shown in *Figure 14a* have uniform thickness, and are principally oriented with their long axis perpendicular to the machine direction. The TEM micrograph of the highest oriented sample, A10, of the films made from Resin 1 is shown in *Figure 17*. More 'corrugated' lamellae are observed in *Figure 17*. Since sample A10 clearly has a greater f_c than A1, comparing the analysis of the TEM results with those of WAXS implies that polymer chain is somewhat tilted in the crystalline lamellae of sample A10, which has been reported in many other studies[59–62]. The fibril nuclei which have been accepted as a common feature for extruded film were not observed for either of the samples made from Resin 1. There is also no clear sign of lamellae twist in the extruded films made from Resin 1, which leaves the small amount of a-axis orientation along the MD an unsolved problem.

The TEM micrographs of the lowest and highest oriented samples of the films made from Resin 2 are

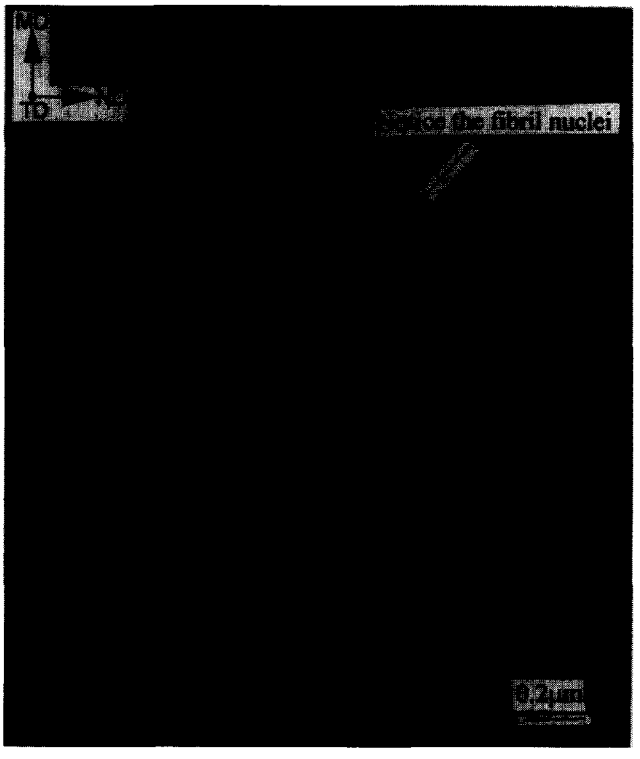

Figure 19 The TEM micrograph of the highest oriented Resin 2 film—sample B11

shown in *Figures 18* and *19*. Interestingly, row nucleated structure were distinctly found for the samples made from Resin 2 but for none of the samples made from Resin 1 under this range of process conditions. This may not be particularly surprising since broadening the molecular weight distribution at constant $\bar{M}_n$ provides a slower relaxing melt. Hence the higher prominence of row structure for Resin 2 is clearly believed due to the longer melt relaxation behaviour of this material. This statement will be further discussed and confirmed by melt rheological data in a later paper.

It is important to point out that for the earlier presented WAXS diffraction patterns, intense sharp spots were found superimposed on the equatorial (110), (200), and (020) reflections from the samples with fibril nuclei made from Resin 2. Since these nuclei are not within the narrower distribution material, they are not seen in these same reflections for Resin 1. Therefore it is clear that the intense sharp WAXS reflection spots of the samples made from Resin 2 arise from the highly oriented fibril nuclei shown in the TEM micrographs. In this study, it is also clear that two distinct types of morphology are observed by TEM. One is the stacked lamellae for Resin 1 and the other is the row nucleated morphology for Resin 2 and the existence of the latter was confirmed by the WAXS diffraction patterns. It is also important to mention again that the values of $f_{c,WAXS}$ for Resin 2 were determined by WAXS without considering the intense sharp spots on the equatorial (200) and (020) reflections. Since the volume fraction of the actual fibril nuclei observed by TEM in Resin 2 and the crystalline intrinsic birefringence are small, the contribution from the fibril nuclei in Resin 2 to the total birefringence is also very small. As shown in *Figure 6*, both Resin 1 and Resin 2 have similar SAXS profiles which suggest that both resins should possess the same morphology—a well stacked lamellae structure. Hence, the above discussion reveals that SAXS cannot distinguish the difference between Resins 1 and 2 in their morphological characteristics.

The applied stress field has been shown as a very important variable in determining the structure/orientation properties of the extruded tubular films[12]. Since the viscosity of polymer melt increases with decreasing process temperature, lower melt temperature at the die exit will result in a higher line stress and therefore promotes a higher oriented melt. Besides line stress, it is certainly expected that the relaxation of the polymer melt during the cooling process is also extremely important in influencing the structure development in the extruded films. How much orientation can be maintained from the oriented melt into the final product is strongly dependent on how fast and how early the oriented melt is quenched and crystallized. From these considerations one would expect that a smaller quench height can allow the oriented melt to be quenched earlier that the oriented polymer melt can crystallize faster and relax slower. Higher air flow rate can remove the heat from the hot polymer melt more efficiently that it can prevent the relaxation of the oriented melt and so does a faster line speed which leads to a shorter time scale for the hot melt to reach the cooling ring. In this study it has been shown that the orientation function of Resin 2 with a broader molecular weight distribution is less sensitive to the four processing variables than Resin 1 with a narrower molecular weight distribution. Furthermore under the same processing conditions, Resin 2 obtained a higher orientation state than Resin 1 and fibril nucleated structure was induced within Resin 2 but not for Resin 1. In *Table 2*, samples A3 and A5 made from Resin 1 were used to examine the reproducibility of the extrusion process and so were samples B3 and B6 made from Resin 2 in *Table 3*. Since the orientation functions of A3 and A5 in *Table 4* are very close to each other and the orientation functions of B3 and B6 in *Table 5* are identical, it is verified that the extrusion procedures utilized in this study are reproducible with respect to film morphology.

From the analysis of the f_c values for Resin 1 to the four process variables, it was found that the melt temperature at the die exit and quench height have a much greater influence than the quench rate and line speed in determining the orientation state of the extruded films made from Resin 1. If one compares samples A2 and A10, it can be clearly seen that a smaller quench height and lower melt temperature can promote a higher orientation function. These findings suggest that for the processing window utilized in this study, the extruded film, which is quenched earlier during the cooling process, will relax less and therefore gain more orientation. This also suggests that besides line stress, the relaxation mechanism of the oriented melt during the cooling step is a very key point for controlling structure/orientation properties of extruded films and the higher prominence of fibril nucleated structure in Resin 2 with a broader molecular weight distribution is due to the longer relaxation behaviour of this material. In fact, as a result of its longer relaxation behaviour, little dependence on the same range of processing variables that were utilized for Resin 1 was noted.

CONCLUSION

Two different types of morphology were found by TEM for the two HDPE resins processed by uniaxial tubular extrusion. One was the stacked lamellae for Resin 1 and the other was the fibril nucleated structure for Resin 2. The fibril nuclei observed by TEM for Resin 2 with a broader molecular weight distribution were also confirmed by intense sharp equatorial spots superimposed on the WAXS (110), (200), and (020) reflections. The origin of this pronounced fibril nucleated structure was distinctly believed due to the longer melt relaxation time behaviour of Resin 2 during the cooling step of the extrusion process. In contrast to Resin 2, the fibril nuclei were not seen by TEM for Resin 1 nor were any intense sharp equatorial reflections observable in the WAXS diffraction patterns. These observations clearly support the row nucleated model in one way but also question the range of its applicability to crystallization under stress in another aspect. Without considering the expected relaxation behaviour of a polymer melt, the row nucleated model proposed by Keller *et al.* treats 'stress' as the important parameter for determining the structure/orientation behaviour of extruded films. Since the oriented fibril nuclei were not evident by TEM and WAXS for Resin 1 nor was significant lamellae twist as suggested in the row nucleated model for the lowest stress case seen for either of the samples in this work by TEM, it is possible that the 'row nucleated model' may need some further modification to account for the types of morphology discussed within this paper.

From birefringence and *FT*i.r. dichroism analysis, it was found that amorphous orientation is small and the form birefringence effects appear to be unimportant in the extruded tubular films. These findings confirm the observation that the experimentally measured birefringence arose almost exclusively from the crystalline phase. The c-axis (chain axis) f_c values were found to be particularly sensitive to the quench height and melt temperature for Resin 1 with a narrower distribution, but much less so for Resin 2 with a broader distribution. Since the melt rheological behaviour of HDPE strongly depends on its molecular weight distribution, the results presented in this paper suggest that both line stress and the relaxation mechanism of the oriented polymer melt during the cooling process are critical for the structure development in the extruded films. It is believed that the orientation state and morphological features of the extruded films will influence the properties of microporous membranes made from these extruded precursor films by further annealing and stretching processes.

ACKNOWLEDGEMENTS

The authors wish to thank the Hoechst Celanese Corporation for their financial support of this work. In addition we would like to thank Robert W. Callahan and Harold M. Fisher for processing the extruded films and Steve McCartney for his assistance regarding the HSEM analysis.

REFERENCES

1 Holmes, D. R., Miller, R. G., Palmer, R. P. and Bunn, C. W. *Nature* 1953, **171**, 1104
2 Aggarwal, S. L., Tilley, G. P. and Sweeting, O. J. *J. Appl. Polym. Sci.* 1959, **1**, 91
3 Keller, A. *Nature* 1954, **174**, 926
4 Keller, A. *J. Polym. Sci.* 1955, **15**, 31
5 Stein, R. S. and Judge, J. T. *J. Appl. Phys.* 1961, **32**, 2357
6 Lindenmeyer, P. H. and Lustig, S. *J. Appl. Polym. Sci.* 1965, **9**, 227
7 Keller, A. and Machin, M. *J. Macromol. Sci. Phys.* 1967, **B1(1)**, 153
8 Maddams, W. F. and Preedy, J. E. *J. Appl. Polym. Sci.* 1978, **22**, 2721
9 Maddams, W. F. and Preddy, J. E. *J. Appl. Polym. Sci.* 1978, **22**, 2739
10 Maddams, W. F. and Preedy, J. E. *J. Appl. Polym. Sci.* 1978, **22**, 2751
11 Maddams, W. F. and Preedy, J. E. *J. Appl. Polym. Sci.* 1978, **22**, 3027
12 Choi, K., Spruiell, J. E. and White, J. L. *J. Polym. Sci., Polym. Phys. Edn* 1982, **20**, 27
13 Gilbert, M., Hemsley, D. A. and Patel, S. R. *Br. Polym. J.* 1987, **19**, 9
14 Sprague, B. S. *J. Macromol. Sci. Phys.* 1973, **B8(1–2)**, 157
15 Quynn, R. G. and Brody, H. *J. Macromol. Sci. Phys.* 1970, **B4(3)**, 953
16 Isaacson, R. B. and Bierenbaum, H. S. U.S. Pat. 3,558,764, 1971 (to Celanese Corp. U.S.A.)
17 Cannon, S. L., Statton, W. O. and Hearle, J. W. S. *Polym. Eng. Sci.* 1975, **15**, 633
18 Clark, E. S. 'Structure and Properties in Polymer Films' (Eds R. W. Lenz and R. S. Stein), Plenum Press, New York, 1972, pp. 267–282
19 Clark, E. S., *Encycl. Polym. Sci. Eng.* 1988, **5**, 408
20 Park, I. K. and Noether, H. D. *Colloid Polym. Sci.* 1975, **253**, 824
21 Noether, H. D. and Whitney, W. *Kolloid Z. Z. Polym.* 1973, **251**, 991
22 Noether, H. D. *Progr. Colloid Polym. Sci.* 1979, **66**, 109
23 Beyer, R. K. and Sprenger, H. *Rheol. Acta* 1980, **19**, 507
24 Cayrol, B. and Petermann, J. *Colloid Polym. Sci.* 1975, **253**, 840
25 Noether, H. D. *Polym. Eng. Sci.* 1979, **19**, 427
26 Bierenbaum, H. S., Isaacson, R. B., Druin, M. L. and Plovan, S. G. *Ind. Eng. Chem. Prod. Res. Dev.* 1974, **13**, 2
27 Callahan, R. *AICHE Symp.* 1988, **84(261)**, 54
28 Sarada, T., Sawyer, L. C. and Ostler, M. I. *J. Membr. Sci.* 1983, **15(1)**, 97
29 Chen, R. T., Saw, C. K., Jamieson, M. G., Aversa, T. R. and Callahan, R. W. *J. Appl. Polym. Sci.* 1994, **53**, 471
30 Yu, T. H. and Wilkes, G. L. *Polym. Prepr.* 1994, **35(2)**, 785
31 Wilkes, G. L. *Encycl. Polym. Sci. Eng.* 1988, **14**, 542
32 White, J. L. *Encycl. Polym. Sci. Eng.* 1988, **10**, 595
33 Samuels, R. J. 'Structured Polymer Properties', John Wiley & Sons, New York, 1974
34 Stein, R. S. 'Newer Methods in Polymer Characterization', Wiley–Interscience, New York, 1964, Chapter 4
35 Stein, R. S. and Norris, F. H. *J. Polym. Sci.* 1956, **21**, 381
36 Seguela, R. and Rietsch, F. *Polymer* 1986, **27**, 532
37 Volkenstein, M. V. 'Configurational Statistics of Polymeric Chains', Wiley–Interscience, New York, 1963, Chapter 7
38 Mead, W. T., Desper, C. R. and Porter, R. S. *J. Polym. Sci., Polym. Phys. Edn* 1979, **17**, 859
39 Pietralla, M., Grossman, H. P. and Kruger, J. K. *J. Polym. Sci., Polym. Phys. Edn* 1982, **20**, 1193
40 Stein, R. S. *J. Polym. Sci.* 1958, **31**, 327
41 Stein, R. S. *J. Polym. Sci.* 1958, **31**, 335
42 Stein, R. S. and Suthkrland, G. B. B. M. *J. Chem. Phys.* 1953, **21**, 370
43 Keller, A. and Sandeman, I. *J. Polym. Sci.* 1954, **71**, 511
44 Read, B. E., 'Structure and Properties of Oriented Polymers' (Ed. Ward, I. M.), John Wiley & Sons, 1975, Chapter 4
45 Read, B. E. and Stein, R. S. *Macromolecules* 1968, **1**, 116
46 Myers, C. W. and Cooper, S. L. *Appl. Spectrosc.* 1994, **48(1)**, 72
47 Glenz, W. and Peterlin, A. *J. Macromol. Sci. Phys.* 1970, **B4(3)**, 473
48 Glenz, W. and Peterlin, A. *J. Polym. Sci.: A-2* 1971, **9**, 1191
49 Garber, C. A. and Clark, E. S. *Int. J. Polym. Mater.* 1971, **1**, 31
50 Quynn, R. G. and Brody, H. *J. Macromol. Sci. Phys.* 1971, **B5(4)**, 721
51 Cannon, S. L., McKenna and Statton, W. O. *J. Polym. Sci.: Macromol. Rev.* 1976, **11**, 209
52 Keller, A. and Kolnaar, J. W. H. *Progr. Colloid Polym. Sci.* 1993, **92**, 81

53 de Gennes, P. G. *J. Chem. Phys.* 1974, **60**, 15
54 Bettelheim, F. A. and Stein, R. S. *J. Polym. Sci.* 1958, **27**, 567
55 Mandelkern, L. 'Crystallization of Polymers', McGraw Hill, New York, 1964
56 Grubb, D. T. and Keller, A. *J. Polym. Sci., Polym. Phys. Edn* 1980, **18**, 207
57 Misra, S., Lu, F. M., Spruiell, J. E. and Richeson, G. C. *J. Appl. Polym. Sci.* 1995, **56**, 1761
58 Park, I. K. and Noether, H. D. *Colloid Polym. Sci.* 1975, **253**, 824
59 Keller, A. and Pope, D. P. *J. Mater. Sci.* 1971, **6**, 453
60 Hay, I. L. and Keller, A. *J. Mater. Sci.* 1966, **1**, 41
61 Hay, I. L. and Keller, A. *J. Mater. Sci.* 1967, **2**, 538
62 Song, H. H., Argon, A. S. and Cohen, R. E. *Macromolecules* 1990, **23**, 870